Journal of Polymer Science

WILEY

JOURNAL OF POLYMER SCIENCE

RESEARCH ARTICLE OPEN ACCESS

Development and Characterization of Lignin-Based Hydrogels for Efficient Adsorption of Diclofenac From Aqueous Environment

Simone Ranieri[1] | Michela Pisani[1] | Francesca Luzi[1] | Marco Parlapiano[1] | Elisabetta Giorgini[2] | Marco Rallini[3] | Valeria Corinaldesi[1] | Paola Astolfi[1]

[1]Department of Science and Engineering of Materials, Environment and Urban Planning—SIMAU, Polytechnic University of Marche, Ancona, Italy | [2]Department of Life and Environmental Sciences—DISVA, Polytechnic University of Marche, Ancona, Italy | [3]Department of Civil and Environmental Engineering, University of Perugia, UdR INSTM, Terni, Italy

Correspondence: Michela Pisani (m.pisani@univpm.it)

Received: 7 May 2025 | **Revised:** 2 July 2025 | **Accepted:** 7 July 2025

Funding: This work was supported by European Union-NextGenerationEU - Project Vitality—Project Code ECS00000041, CUPI33C22001330007—funded under the National Recovery and Resilience Plan (NRRP).

Keywords: diclofenac adsorption | kinetics and adsorption isotherms | lignin hydrogels

ABSTRACT

Hydrogels are interesting materials with potential applications in the treatment of water contaminated by organic and inorganic toxic compounds. Among the different monomers/polymers commonly used, the natural polymer lignin is undoubtedly an attractive candidate due to its biocompatibility, biodegradability, low toxicity, and availability in high quantities as the main by-product of the pulp industry. In the present work, the synthesis and characterization of a lignin-based hydrogel are described and tested in the adsorption of the nonsteroidal anti-inflammatory drug, diclofenac, one of the so-called emerging contaminants. Due to the anionic nature of diclofenac currently used in pharmaceutical preparations, a cationic functionality is included in the polymeric backbone. The obtained hydrogel is characterized by a porous structure, thermal stability, and an elastic behavior more pronounced than the viscous one. It has a high swelling capacity and is able to efficiently remove diclofenac in batch mode, following a pseudo-second order kinetic, and adsorption could be well described by Langmuir and Sips isothermal models. For the first time, diclofenac removal by a lignin-based hydrogel is also carried out in a packed-bed column with a maximum capacity of ca. 50 mg/g, and different theoretical models are used to fit the experimental data.

1 | Introduction

The rapid growth of urban areas and industrial activities over the past few decades has significantly contributed to environmental issues, particularly water pollution with a consequent decline of water quality due to the presence of contaminants of emerging concern (CECs) such as inorganic heavy metals and organic chemicals (pesticides, dyes, pharmaceuticals, etc.). Although pharmaceuticals are found in relatively low concentrations (ng-mg/L), their continuous release in the environment could result in long-term exposure of aquatic organisms with consequent toxicity and harmful effects. For this reason, pharmaceuticals have been added to the evolving "watch-list" under the EU Water Framework Directive [1]. Among these, ibuprofen, naproxen, ketoprofen, and diclofenac are non-steroidal anti-inflammatory drugs (NSAIDs) largely used because of their multiple activities (anti-inflammatory, pain-relieving, and antipyretic), but characterized by a

particular stability and resistance to biodegradation and hence ecotoxicity and potential threat to the environment [2]. Consequently, removing pharmaceutical contaminants from water is of paramount importance, requiring the development of effective and sustainable treatment methods. Photocatalytic degradation, biofiltration, chlorination, advanced oxidative processes, electro-coagulation, and adsorption are available techniques [3] for the removal of these pollutants during wastewater treatment, and adsorption is undoubtedly the simplest one, which still guarantees effectiveness and easy pollutant removal [4]. Adsorbent materials can be easily regenerated and recycled, thus reducing both the cost of the process and the production of waste materials. Different adsorbents, from diverse origins, have been exploited for the removal of pharmaceutics, and NSAIDs in particular, from wastewater and effluents: activated carbons [5–7], graphene-based materials [8], silica and zeolites [9], metal organic frameworks [10, 11], biochars [12, 13] obtained by the pyrolysis of biomass wastes, and various kinds of polymers such as molecularly imprinted polymers [14, 15]. Among these, special attention is deserved to hydrogels, crosslinked polymers characterized by a stable 3D structure able to absorb large amounts of water and swell their original volume over multiple cycles. It is their high-water adsorption capacity that determines the characteristics of these materials, such as permeability, elasticity, and flexibility. Hydrogels can be synthesized starting from many types of monomers, petroleum-based such as acrylic acid, acrylate derivatives, and vinyl alcohols, or natural such as cellulose, chitosan, lignin, starch, or a combination of both, and can also be functionalized to increase their adsorption capacity. Lignin is an ideal material to be used for this purpose, being the second most abundant natural polymer on earth, bio-renewable, nontoxic, eco-friendly, biodegradable, and frequently available in high quantities as a main byproduct of the pulp indust6ry. Moreover, lignin can be considered a versatile material and a sustainable feedstock for functional materials as in the case of lignin pyrolysis to produce monophenolic chemicals and other carbon-based adsorbents [16]. However, due to its aromatic structure consisting of three cross-linked aromatic units called "lignols" (coniferyl, sinapyl, and coumaryl alcohols), lignin is rather hydrophobic, and for this reason, it is rarely used alone in hydrogel preparation. However, it has the advantage to be easily grafted or combined with other hydrophilic substances, thus obtaining lignin-based composite hydrogels that can be used in several fields, from biomedical to environmental applications [17]. Lignin-based hydrogels, due to their porous structure and the presence of several oxygen-containing groups as possible active sites, have been prepared and used in water treatment for the removal of pollutants, specifically heavy metals and organic dyes, from water and wastewater [18, 19], whereas no reports can be found in the literature on the application of these kinds of hydrogels for NSAIDs adsorption. In this context, a cationic hydrogel (LS-pAAm-DAC) was prepared by copolymerization of lignin sulfonate (LS) with acrylamide (AAm) including in the polymeric backbone also an acryloyloxy derivative with a cationic amino group, and characterized. The swelling and deswelling capacities of the prepared hydrogel were investigated and, for the first time, its adsorption performance toward diclofenac (DCF-Na), one of the most common anti-inflammatory drugs and hence also one of the most highly detected in wastewater, was tested.

2 | Experimental Section

2.1 | Materials

LS, N,N′-Methylenebisacrylamide (MBAAm), AAm, potassium persulfate (KPS), tetramethylethylenediamine (TEMED), [2-(Acryloyloxy)ethyl]trimethylammonium chloride (80 wt% solution in water) (DAC) and Diclofenac Sodium (DCF-Na) were purchased from Merck and used as received. Ultrapure water (Younglin aqua Max Ultra 370) was used as the solvent in hydrogel synthesis and to prepare every solution employed in all the experiments.

2.2 | Synthesis of LS-pAAm-DAC Cationic Hydrogel

The crosslinked lignin-based hydrogel was prepared by radical polymerization following a procedure already described in the literature [20] with slight modifications. Briefly, LS was dissolved in 20 mL of water (20 mg/mL) together with AAm (1400 mg, 20 mmol) and MBAAm (36 mg, 0.23 mmol) and stirred at 300 rpm and 30°C for 30 min. Then, KPS (220 mg, 0.8 mmol) was added to the reaction mixture, and the temperature was raised to 40°C, followed by the addition of TEMED (70 μL, 0.5 mmol) and DAC (770 μL, 3.6 mmol). After 30 min, the gel formation was observed, but the system was left in this condition for 4 h to complete the reaction. At the end of the synthesis, the hydrogel was thoroughly washed and rinsed with water and acetone to remove unreacted monomers and used in this hydrated form for thermal and rheological analyses. For all other characterizations and batch experiments, the hydrogel was firstly frozen at −80°C for 4 h and then freeze-dried at −40°C for 48 h in a Superco Engineering Proxima (Germany) lyophilizer in autodrying mode with a vacuum of 0.38 mbar. A pAAm hydrogel was also prepared by reacting AAm and MBAAm with KPS in the same conditions as described above and used as a reference in the characterization measurements.

2.3 | Hydrogels Characterization

Attenuated total reflectance-Fourier transform infrared spectroscopy (ATR-FTIR) spectra were acquired by a platinum ATR accessory mounting a diamond crystal and coupled with a Bruker INVENIO-R interferometer and a Deuterated TriGlycine Sulfate (DTGS) detector (Bruker Optics, Ettlingen, Germany). Few mg of each sample were deposited onto the clean diamond crystal, and ATR-FTIR spectra were collected at room temperature. The following setup was used for all the samples and for background: 4000–400 cm^{-1} spectral range, 128 scans, and 4 cm^{-1} spectral resolution. The measurements were performed in triplicate. IR spectra were vector normalized in the full spectral range (OPUS 7.5, Bruker Optics, Ettlingen, Germany).

The surface morphology of the freeze-dried hydrogels was analyzed by field emission scanning electron microscopy (FE-SEM) using a Zeiss Supra 40-VP high vacuum FE-SEM (Germany) microscope. The sample was deposited on conductive carbon adhesive tape, and metallization with gold by sputtering was carried out. The micrographs were acquired by

means of an SE2 detector with an electron high tension (EHT) of 5 kV.

Thermogravimetric analysis (TGA) of pAAm and LS-pAAm-DAC systems was carried out using a Mettler Toledo TGA/SDTA 851 by heating the freeze-dried materials from room temperature (RT) up to 600°C at 10°C/min under nitrogen flow (60 mL/min). Thermograms (TG) and their derivative curves (DTG) obtained from TGA measurements provide the information related to the thermal stability of the materials. The second degradation temperature (T_{dIImax}, maximum value of the second degradation step), the third degradation rate temperature ($T_{dIIImax}$, maximum value of the third degradation step) and the residual mass at 600°C were obtained from the weight loss and its derivative curve.

Differential scanning calorimetry (DSC) tests were carried out with a Seiko EXSTAR 6000 calorimeter, performing two heating and one cooling scans from 30°C to 205°C for pAAm and from 30°C to 195°C for LS-pAAm-DAC at 10°C/min under a nitrogen flow rate of 50 mL/min. The thermal analysis was carried out using freeze-dried polymeric systems.

The viscoelastic properties of pAAm and LS-pAAm-DAC hydrogels were investigated by using a MCR 702e Anton-Paar rheometer (Graz, Austria). The tests were performed using plane–plane geometry (upper plate diameter of 25 mm, 1 mm gap and 50 mm lower measuring plate). The dynamic oscillatory measurements were carried out at a constant temperature of 25°C. The samples were swollen in deionized water before analysis and loaded onto the Peltier plate to cover the surface area of the parallel plate. Three measurements of amplitude sweep, frequency sweep, and temperature ramp have been performed for each formulation in this set of experiments. The amplitude sweep was obtained at a constant frequency mode of 10 rad/s over a strain rate range (γ) of 0.01%–100%. The oscillatory shear measurements for frequency sweep tests were performed as a function of the oscillation frequency (ω), from 0.1 to 100 rad/s, for a constant of 1% (in the linear range of viscoelasticity). The storage (G′) and loss (G″) moduli were determined in oscillatory shear conditions as a measure of the stored and dissipated energy during one cycle of deformation, respectively. The loss tangent ($\tan\delta = G''/G'$) gives information about the viscoelastic character of the samples. The temperature ramp was recorded at a constant strain rate of 1%, with a low frequency of 10 rad/s over a temperature range of 5°C–50°C. The temperature ramp rate was 5°C/min. Frequency and temperature ramp tests were conducted with the humidity constantly set at 80%.

2.4 | Swelling and Deswelling Properties

Swelling and deswelling abilities of the LS-pAAm-DAC hydrogel were determined gravimetrically. Small pieces of freeze-dried hydrogels were accurately weighed and immersed in water to swell until equilibrium at room temperature. The swelling degree was determined by weighing the swollen hydrogels at regular time intervals after having removed the excess of water on the surface with filter paper. The swelling degree was calculated according to the following Equation (1):

$$S(\%) = \frac{M_t - M_0}{M_0} * 100 \quad (1)$$

where M_0 and M_t are the weights of the dry gel and the swollen gel at time t, respectively.

For deswelling measurement, hydrogels were swelled to equilibrium in ultrapure water and then allowed to air dry at room temperature and weighed at regular intervals. Once weight changes were no more observed between the measurements, water retention (WR%) was calculated according to Equation (2):

$$\mathrm{WR}(\%) = \left(1 - \frac{M_t - M_0}{M_e - M_0}\right) * 100 \quad (2)$$

where M_0 is the weight of the dried hydrogel, M_e and M_t are the weights of the swollen gel at equilibrium time and at time t, respectively [21].

2.5 | DCF-Na Removal: Batch Experiment

Adsorption of DCF-Na by LS-pAAm-DAC hydrogel was studied in batch mode. Fixed masses of hydrogel (100 mg) were immersed in 50 mL of DCF-Na aqueous solutions at different concentrations (15, 30, 60, 80, and 125 mg/L) and left on an orbital shaker at 150 rpm at room temperature for 420 min. DCF-Na concentration in the supernatant was determined by UV–Vis spectroscopy at 276 nm (Microplate Synergy HT, Biotek, Winooski, VT, USA) at regular time intervals (15 min for the first 2 h and then 30 min for the following time) and by using a calibration curve for DCF-Na in the concentration range 0.5–125 mg/L. Measurements were all performed in triplicate on three independent samples.

A sample of LS-pAAm-DAC hydrogel used for DCF-Na adsorption was freeze-dried again and analyzed by SEM and ATR-FTIR.

2.6 | DCF-Na Removal: Packed-Bed Column

250 mg of dried hydrogel was placed in a column with an inner diameter of 1.25 cm and left to swell in water overnight. The adsorption experiments were conducted in spiked ultrapure water with DCF-Na salt 50 mg/L. The solution was passed through the column upward with a peristaltic pump (Gilson Minipuls 3) at a flow rate of 0.625 mL/min. The bed height of the column was 4.0 cm with a consequently empty bed contact time (EBCT) of 7.6 min. Samples were collected every 20 min, and the concentration of DCF-Na was measured by UV–Vis spectroscopy at 276 nm.

3 | Results and Discussion

A lignin-based hydrogel was prepared in the present work by radical polymerization, using potassium persulfate as a water-soluble radical initiator, as it efficiently generates sulfate radical under moderate thermal conditions (approximately 40°C), thereby helping to preserve the structural integrity of organic components. Moreover, KPS is less toxic, more cost-effective,

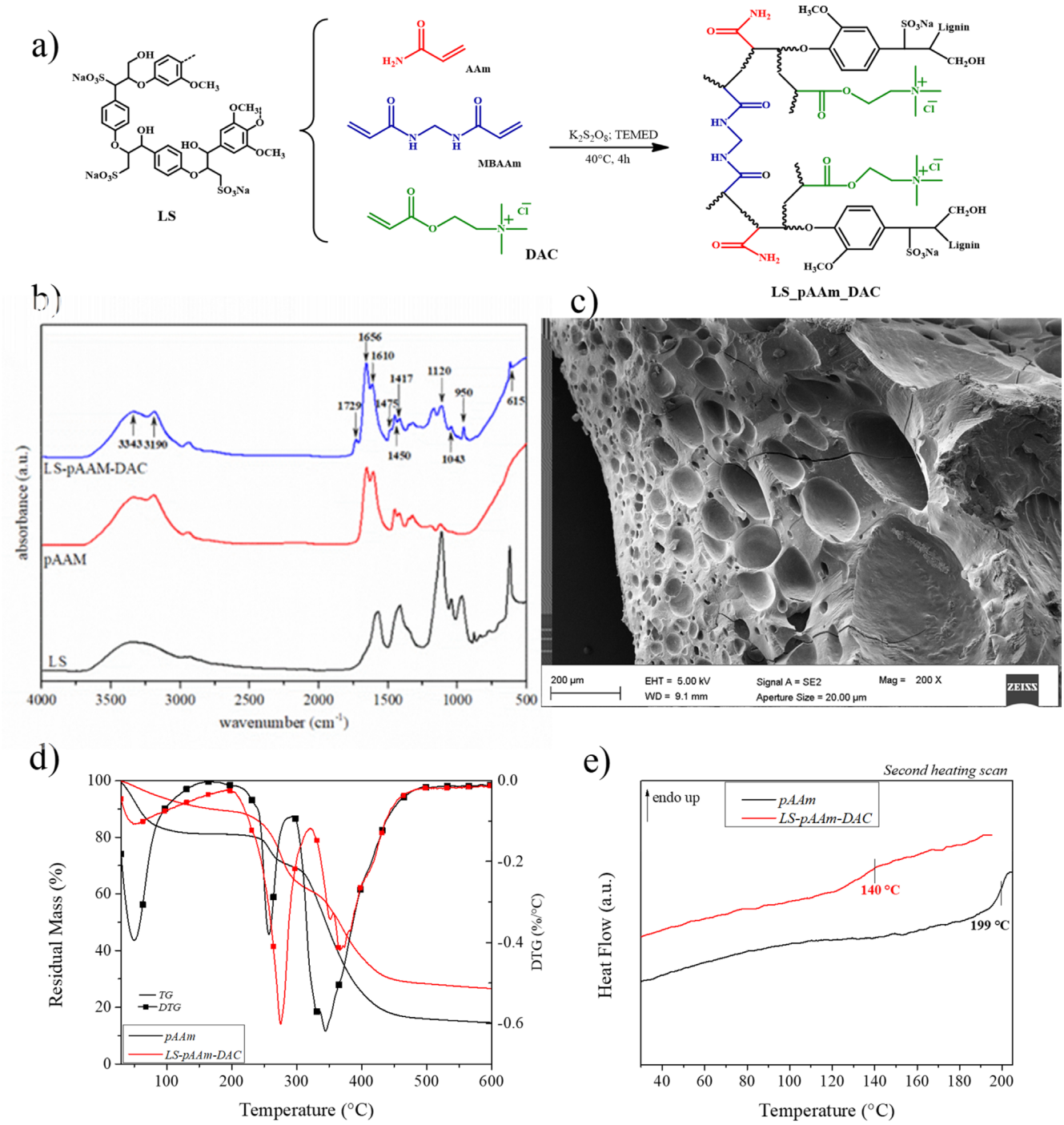

FIGURE 1 | (a) Synthesis of LS-pAAm-DAC hydrogel; (b) ATR spectra of LS (black line), pAAm (red line) and LS-pAAm-DAC (blue line); (c) FESEM image of hydrogel LS-pAAm-DAC; (d) residual mass (TG) and differential residual mass (DTG) of pAAm and LS-pAAm-DAC polymeric formulations; (e) DSC thermograms at the second heating scan for pAAm and LS-pAAm-DAC.

and easier to handle compared to commonly used water-soluble initiators such as 2,2′-Azobis[2-(2-imidazolin-2-yl)propane] dihydrochloride (AIBA) or 4,4′-Azobis(4-cyanopentanoic acid) (ACPA) [22]. Different types of lignin products are available according to the manufacturing processes, such as sulfonate lignin, obtained in the sulfite pulping process, used in the present work and chosen for its water solubility. Thanks to the phenolic —OH groups present in the lignin macromolecule, phenoxyl radicals are formed and readily react with AAm and/or MBAAm monomers or propagated monomers to form a grafted network (Figure 1a) [20, 23]. Moreover, the cationic monomer DAC was included in the synthesis to introduce a cationic functionality in the polymer structure, which may be particularly useful in the wastewater treatment field since many CECs, such as DCF considered in the present work, are present in the aqueous environment as anionic compounds.

3.1 | Hydrogel Characterization

ATR spectra of LS-pAAm-DAC are shown in Figure 1b, with those of LS and pAAm reported for comparison. In the

LS-pAAm-DAC spectrum, some characteristic bands of pAAm and DAC are clear, thus confirming the successful grafting onto lignin. Moreover, for pAAm, the following bands were found: ~3343 and ~3190 cm^{-1} (asymmetric and symmetric stretching of N—H); ~1656 cm^{-1} (stretching of C═O amide); ~1610 cm^{-1} (bending of N—H); ~1450 cm^{-1} (deformation of CH_2 moieties); and ~1417 cm^{-1} (stretching C—N and deformation of N—H and C—H). Noteworthy is a small peak at ~1729 cm^{-1} (stretching vibration of the C═O ester moiety) and the peaks at ~1475 and ~950 cm^{-1} (respectively stretching and bending vibrations of the quaternary ammonium group) [24, 25] suggest the presence of DAC functional groups in the hydrogel structure. Finally, the presence of lignin is confirmed by the peaks at ~1120 cm^{-1} (stretching of C—O), ~1043 cm^{-1} (stretching of S═O), and ~615 cm^{-1} (stretching of S—O) [20].

In SI (Figure S1) ATR spectra of LS-pAAm-DAC before and after DCF-Na removal are shown, and the presence of some characteristic peaks of DCF-Na confirms the adsorption of the contaminant.

The morphology of the freeze-dried prepared LS-pAAm-DAC hydrogel was characterized by FESEM (Figure 1c). The hydrogel surface showed a three-dimensional highly microporous network structure, with interconnected pore distribution ranging from a few to tens of microns. The presence of these pores allows water transport and promotes also the diffusion of water pollutants from the external surface of the hydrogel to the interior, making this material a good candidate for water remediation applications. The hydrogel interpenetrating network channels did not change in size and shape after DCF-Na adsorption (Figure S2).

The thermal properties of pAAm and LS-pAAm-DAC based polymeric hydrogels were investigated by TGA and DSC. The differential scanning calorimetry was used to determine the glass transition temperatures (T_g) of synthesized polymeric systems.

In Figure 1d, the residual mass (TG) and derivative (DTG) curves for pAAm and LS-pAAm-DAC polymeric systems are reported, and a multistep degradative behavior is clear for the two polymeric systems [26–28]. The first stage of degradation and the corresponding mass loss below 100°C is due to the evaporation of water or moisture absorbed by the polymer systems [26, 28], and is indicative of the hygroscopic nature of the analyzed formulations. In the second region around 200°C–300°C, pAAm based systems undergo irreversible degradation processes related to intra- and intermolecular imidization reactions at the amide group and to thermal decomposition of methyl groups from quaternary ammonium [29]. As reported in the literature the second thermodegradative peak is associated with the release of NH_3, H_2O, and minor quantities of CO_2 [30]. The third degradation peak is centered at 300°C–500°C; in this thermal condition, imides begin to decompose, forming CO_2 and H_2O. In this thermal region, previously formed cyclic imides break down and, as a result, random cleavages of the main polymer chain occur with the formation of glutarimides [30]. Moreover, in LS-pAAm-DAC an improvement in thermal stability was observed, together with a shift to higher temperatures of the second (from $T_{dII\ pAAm}$ = 257°C to $T_{dII\ LS\text{-}pAAm\text{-}DAC}$ = 275°C) and third thermodegradative peaks (from $T_{dIII\ pAAm}$ = 343°C to $T_{dIII\ LS\text{-}pAAm\text{-}DAC}$ = 367°C) [26]. A similar consideration can be made for the $T_{onset\ IIId}$ main peak (onset of the third degradation rate temperature) that shifted to a higher temperature with the addition of LS during the reaction in polymeric-based systems. Finally, an increase in the residual mass values at 600°C for LS-pAAm-DAC (around 16%) when compared to pure pAAm (around 15%) is observed and induced by the presence of the LS. These data agree with the literature [26].

Figure 1e shows DSC thermal curves of polymeric systems during the second heating scan. The glass transition of pAAm is centered at 199°C, as also reported by Silva et al. [31]. The high value of T_g for pAAm underlines the crosslinked nature of the polymer as a result of the presence of the functional group N,N′-methylenebisacrylamide in the chemical structure of LS-pAAm-DAC [32].

A decrease in T_g for LS-pAAm-DAC (140°C) was registered likely due to the presence of the cationic acryloyloxy derivative. In fact, such a considerable shift was not observed in an LS-pAAm system (data not shown).

The viscoelastic properties of LS-pAAm-DAC were determined and compared with those of pAAm hydrogel, as shown in Figure 2. The viscoelastic parameters are determined by means of different tests. Initially, an amplitude test is performed for the evaluation of the % strain, linear viscoelastic range (LVE), and structural strength at 25°C. The storage (G′) and loss (G″) moduli against the % strain are determined in the range from 0.01% to 100%. In Figure 2a the viscoelastic parameters, storage and loss moduli (G′ and G″, respectively), are plotted as a function of shear strain (γ) for pAAm and LS-pAAm-DAC hydrogels. G′ was higher than G″ over the whole shear strain range of analysis, in agreement with the literature [23], reflecting that the systems (in the range of analysis) are characterized by higher elastic than viscous behavior. A constant plateau was observed for the G′ value within the LVE region with G′ > G″, both samples have a solid structure (up to the value of γ = 10%). Initially, the hydrogels demonstrated that the moduli were independent of shear strain, displaying linear viscoelastic behavior (solid-like) [33]. The LVE regime is fixed at 1% of strain; after that, a slight deviation of G′ was observed. The maximum storage modulus in the linear viscoelastic region was observed at 4200 and 2300 Pa for pAAm and LS-pAAm-DAC based systems, respectively. Moreover, a reduction in the storage and loss moduli was observed in LS-pAAm-DAC compared to pAAm after the introduction of LS and cationic acryloyloxy derivative in the polyacrylamide (pAAm) backbone. At high shear strain (γ = 100%) values, the LS-pAAm-DAC hydrogel exhibited a phase change from primarily elastic to primarily viscous behavior.

The dependences of the viscoelastic parameters G′, G″ and tanδ on the oscillation frequency (ω) for pAAm based formulations are shown in Figure 2b,c, respectively. In the frequency sweep test, both the hydrogels have a behavior similar to that observed in the amplitude sweep analysis: from 0.1 to 100 rad/s and for a constant strain (γ) of 1%, the elastic modulus (G′) (Figure 2b) presents higher values than the viscous modulus (G″). The elastic (G′′) and viscous (G″) moduli remain constant in the selected frequency range and consequently also the tanδ is constant for both polymeric systems.

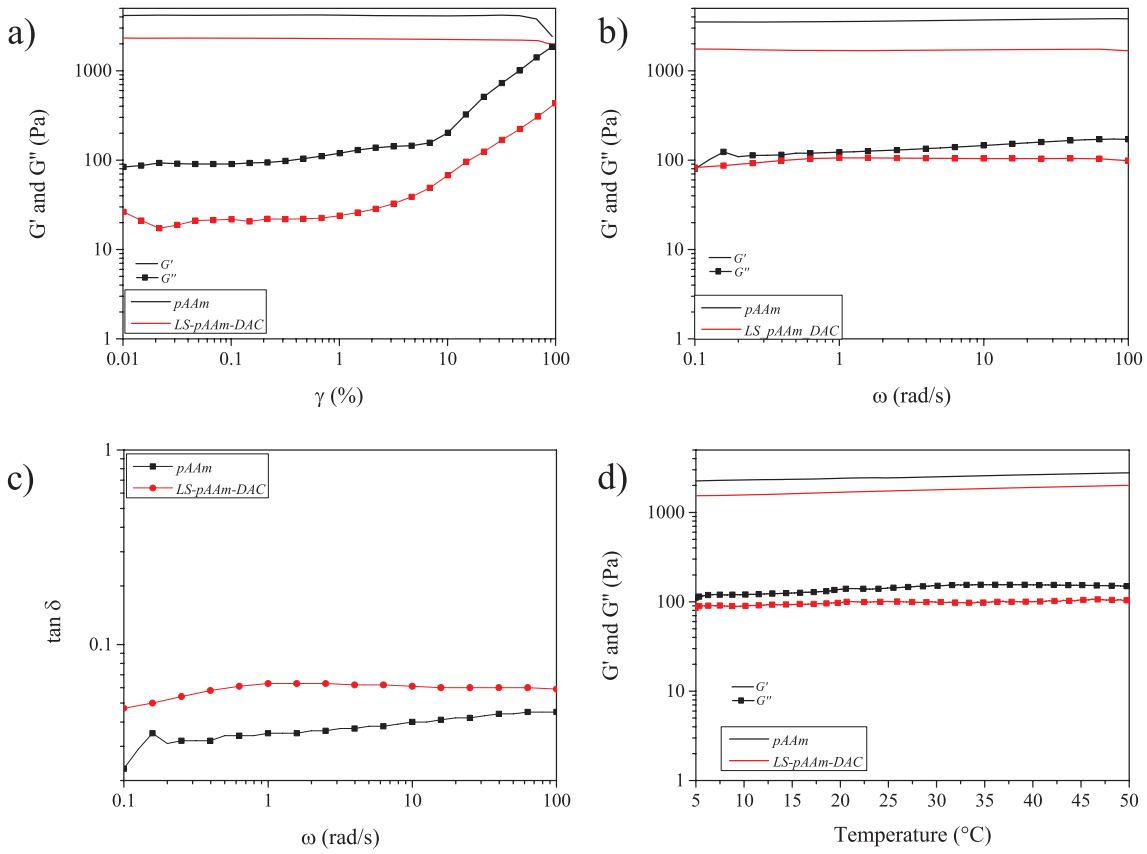

FIGURE 2 | (a) Strain amplitude sweep of pAAm based hydrogels; (b) variation of G' and G″ as a function of ω for pAAm and LS-pAAm-DAC; (c) variation of tanδ as a function of ω for pAAm and LS-pAAm-DAC; (d) temperature ramp of pAAm and LS-pAAm-DAC.

The consistent behavior of the moduli, with no significant variations, indicates that the material remains stable throughout the test. For both hydrogels, the fact that G′ exceeds G″ suggests their high elastic nature [33]. Furthermore, the higher values of G′ and G″ for pAAm respect to LS-pAAm-DAC, supporting the amplitude sweep test results and indicating the high viscoelastic and mechanical properties of pAAm based system, that can be related to the physical interaction points among the polymer molecules [34].

The loss tangent values (tanδ), representing the ratio of G″ to G′ (indicating the viscoelastic character of the materials), were plotted against frequency in Figure 2c. The tanδ values <1 underline the viscoelastic nature of both the hydrogels.

Recent advances in ionic conductive hydrogels have demonstrated how tunable viscoelasticity can enable multifunctional applications, such as self-healing sensors [35]. While our lignin-based hydrogel prioritizes adsorption capacity, future iterations could explore similar conductive or self-repairing properties for expanded functionality. However, pAAm formulation demonstrates a more elastic nature than LS-pAAm-DAC in low and high-frequency regions.

Figure 2d shows the behavior of the viscoelastic parameters G′, G″ at different temperatures. The temperature ramp test confirms the behavior evidenced in the amplitude and frequency tests, with $G' > G''$. Furthermore, pAAm shows higher elastic and viscous moduli respect to LS-pAAm-DAC. The constancy of storage and loss moduli parameters from 5°C to 50°C highlights the possibility of efficiently using these polymeric formulations as stable absorbing materials for removing pharmaceutical contaminants from water in the selected thermal range, without showing differences in the viscoelastic mechanical response. Future modifications could incorporate stimuli-responsive elements, as demonstrated in dual-sensitive hydrogels with tunable adhesion and antibacterial properties, to expand functionality for specific water treatment scenarios [36].

3.2 | Swelling and Deswelling Behavior

The swelling capacity of a hydrogel is one of the most important parameters to be considered for its possible application as an adsorbent, and it depends on many factors: the nature of the polymers used in the synthesis (possible charge, ionic content, crosslinking agent content) and the environmental conditions (pH and temperature of the medium).

The equilibrium swelling ratio of LS-pAAm-DAC in water (pH = 7), calculated through Equation (1), is plotted in Figure 3 as a function of the immersion time: a rapid swelling was achieved in the first hour with almost 800% swelling, and it continued to increase in a slower manner in the following 5 h, then reaching equilibrium. No significant differences were observed in the hydrogel weight after 24 h. Concerning the possibility of reusing hydrogels as water-absorbing materials, their deswelling capabilities are important as well. The water retention curve

for LS-pAAm-DAC is shown in the inset of Figure 3 and was obtained by measuring the mass of each sample left in the air at regular time intervals. The proposed hydrogel tends to release water and to deswell slowly in the first hours, and this may likely be due to the presence of strong interactions between the polar and/or ionic groups in the hydrogel matrix and the water molecules.

3.3 | DCF-Na Removal: Batch Experiments

The effect of DCF-Na concentration on adsorption capacity (q_t) and removal efficiency of LS-pAAm-DAC was determined at five different concentrations in the range 15–125 mg/L, and the obtained results are shown in Figure 4a,b, respectively. As shown in Figure 4a, the adsorption capacity per unit mass (q_t) rapidly increased in the first 45 min for all concentrations tested, followed by a slower increase until a plateau was reached (180–200 min, q_e), with longer equilibrium times for the highest concentrations. Initially, all active sites on the adsorbent surface are unoccupied, and the concentration of DCF-Na in the solution remains high. Consequently, DCF-Na is rapidly adsorbed by the hydrogel, leading to a sharp increase in the adsorption capacity (q_t). As adsorption progresses, the available active sites on the hydrogel become progressively saturated, and the concentration gradient between the solution and the hydrogel surface diminishes, resulting in a slower rate of increase in q_t.

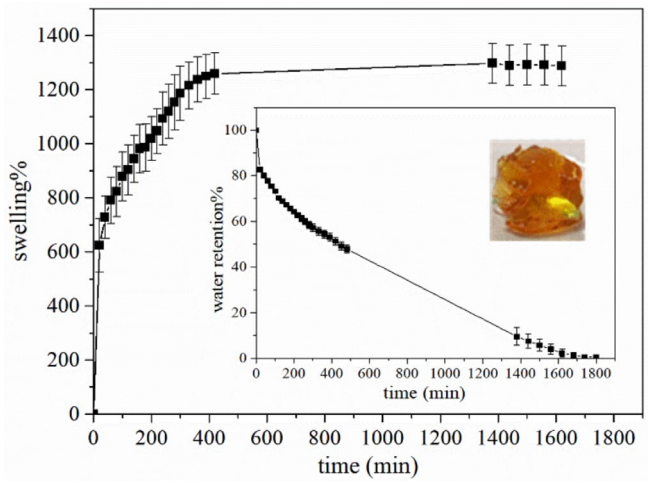

FIGURE 3 | Swelling behavior of lyophilised LS-pAAm-DAC hydrogel in ultrapure H_2O; in the inset, water retention % of the same sample left in open air and an image of the swollen hydrogel.

The adsorption capacity at equilibrium(q_e) was thus determined, and it was found that q_e increased with DCF-Na concentration, as shown in Figure 4b. In fact, q_e increased from ~4 mg/g for 15 mg/L DCF-Na to ~29 mg/g at the highest DCF-Na concentration (125 mg/L), as a consequence of a reduction in the mass transfer resistance at high contaminant concentrations favoring the adsorption process and hence the amount of adsorbed DCF-Na [37]. In the same graph, the removal efficiency (*RE%*) toward DCF-Na was also plotted as a function of DCF-Na concentration, and it was shown that *RE%* decreased with DCF-Na concentration. This behavior may be attributed to the fact that hydrogel samples immersed in solutions with varying DCF-Na concentrations had identical weights, and thus an equal number of potential adsorption sites. At low DCF-Na concentrations, the ratio of the active sites on the hydrogel matrix to DCF-Na molecules is high, allowing for rapid and efficient adsorption, as reflected by high RE% values. Conversely, at higher DCF-Na concentrations, the adsorption sites become saturated, leading to a decrease in *RE%*.

3.4 | Adsorption Kinetics

Determination of adsorption kinetics represents a key step in the evaluation of the efficiency of the hydrogel and allows describing the mechanisms involved in the adsorption process through the formulation of theoretical models. Three different models are commonly used to express adsorption kinetics, namely pseudo-first order (PFO), pseudo-second order (PSO) and intraparticle diffusion [38].

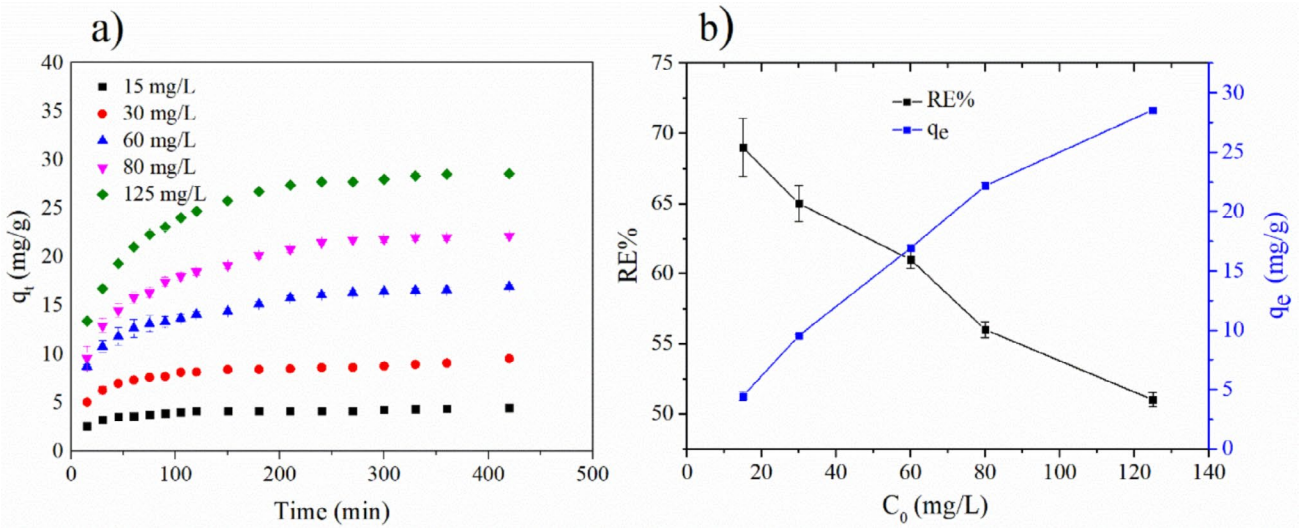

FIGURE 4 | (a) Adsorption capacities (q_t) of DCF-Na by LS-pAAm-DAC hydrogel over time, at different DCF-Na concentrations; (b) effect of DCF-Na concentration on removal efficiency % and on equilibrium adsorption capacities.

TABLE 1 | Kinetics parameters for the adsorption of DCF-Na at different concentrations.

C_0 (mg/L)	15	30	60	80	125
$q_{e,exp}$ (mg/g)	4.45	9.53	16.93	22.16	28.56
Pseudo second order					
$q_{e,cal}$ (mg/g)	4.49	9.54	17.77	23.85	30.40
k_2 (g/(mg min))	0.01566	0.005294	0.002179	0.001373	0.001291
R^2	0.999	0.997	0.998	0.999	0.999
Intraparticle diffusion					
k_{p1} (g/(mg min$^{0.5}$))	0.213	0.470	0.820	1.343	1.665
P_1	1.918	3.529	6.000	5.036	7.559
R_1^2	0.930	0.923	0.945	0.959	0.978
k_{p2} (g/(mg min))	0.00564	0.0862	0.447	0.670	0.680
P_2	4.041	7.252	9.100	11.106	17.39
R_2^2	0.906	0.924	0.980	0.991	0.969
k_{p3} (g/(mg min))	0.0572	0.240	0.154	0.104	0.202
P_3	3.273	4.565	13.729	20.04	24.54
R_3^2	0.958	0.974	0.907	0.946	0.879

According to the first kinetic order model, adsorption rate depends on the diffusion of the adsorbate on the adsorbent surface, meaning that physical adsorption is the dominant process, and the rate constant k_1 (1/min) may be obtained by the linear Equation (3)

$$\log(q_e - q_t) = \log q_e - \frac{k_1 t}{2.303} \tag{3}$$

where t is the adsorption time (min), q_t and q_e are the adsorption capacities (mg/g) at time t and at equilibrium, respectively.

In the pseudo-second kinetic order model, the adsorption process is mainly led by chemical interactions between the adsorbent and the adsorbate. This model can be described in its linear form by Equation (4)

$$\frac{t}{q_t} = \frac{1}{k_2 q_e^2} + \frac{t}{q_e} \tag{4}$$

where the rate constant k_2 is expressed in g/(mg min).

Finally, the intraparticle or internal diffusion model is described by Equation (5)

$$q_t = k_i t^{1/2} + P \tag{5}$$

where the intraparticle diffusion rate constant is k_i in g/(mg min$^{0.5}$) and the constant P is the intercept of the linear regression: if $P = 0$ the rate constant depends only on the intraparticle diffusion; otherwise, the adsorption process depends on multiple steps [39, 40].

In this study, all three models were used to analyze the adsorption kinetic data, but the PFO model gave poor correlation coefficients (R^2) and was not considered. In Table 1, the fitting parameters for the other two kinetic models are reported, and the high values for the correlation coefficient ($R^2 > 0.99$), as shown in Figure S3, suggest that the PSO kinetic model better describes the adsorption behavior of LS-pAAm-DAC toward DCF-Na. Moreover, the calculated equilibrium adsorption capacity (q_e) obtained from the PSO model is in a very good agreement with the experimental one. This supports the hypothesis that chemical adsorption is the dominant mechanism [41], which in the present case may be caused, besides hydrogen bonding and π–π stacking interactions, also by the electrostatic interaction between the quaternary ammonium group (–N$^+$(CH$_3$)$_3$) contained in the LS-pAAm-DAC hydrogel adsorbent and the negative charge of the carboxylate group in DCF-Na (Figure 5). Similar electrostatic interactions and physical entrapment mechanisms have been utilized in various types of charged hydrogels, such as chitosan and alginate, to remove cationic or anionic contaminants, including dyes [42, 43]. Moreover, when considering broader applications, such mechanisms have also been exploited in peptide-based hydrogels for the immobilization of enzymes [44].

As can be observed in Table 1, good correlation coefficients were found also for the intraparticle diffusion model, so this latter model cannot be excluded and may also take place. According to this model [45], the adsorption process can be described by three different steps: [39] the external diffusion (or film diffusion), i.e., the transfer of adsorbate from the bulk solution in the liquid film around the adsorbent; the internal diffusion (or intraparticle diffusion) of the adsorbate through the pores of the adsorbent; and the adsorption

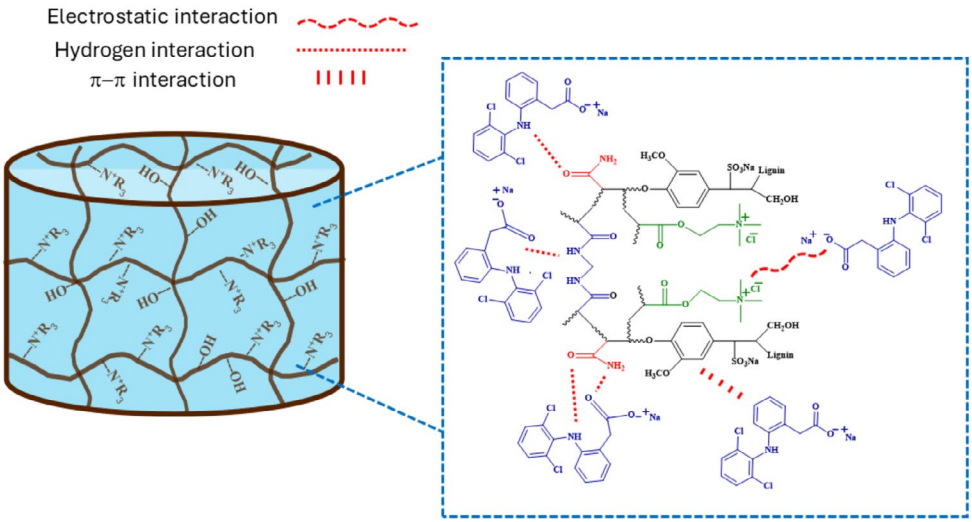

FIGURE 5 | Possible adsorption mechanism of DCF-Na by lignin-based hydrogel based on electrostatic, hydrogen, and π–π interactions.

onto the active sites in the inner and outer surface of the adsorbents. In Figure S4, the three linear regions are visible suggesting that, during adsorption, more than one process simultaneously operates, and, since the intercept $p > 0$, it can be assumed the adsorption process is controlled by multiple steps. This possible multi-step adsorption process aligns with contaminant transport mechanisms in porous media, where anomalous diffusion of contaminants or other substances may occur [46].

3.5 | Adsorption Isotherm

Adsorption isotherm is a valuable tool for studying the adsorption capacity, the surface properties of an adsorbent material, and the interactions between the adsorbate and the adsorbent. In this work, two different isotherm models were applied: Langmuir and Freundlich [14, 47], together with their combination as represented by the Sips model [48].

Langmuir isotherm model assumes a monolayer adsorption on energetically equivalent active sites on the adsorbent. It is based on three assumptions: (a) the solid surface has a finite number of active sites that are energetically equivalent; (b) there are no interactions between the adsorbed species, so the adsorption rate is independent from the absorbate amount; (c) the monolayer is formed when each active site is occupied by one particle.

The Freundlich isotherm model describes adsorption as a multilayer process, with energetically inhomogeneous active sites and interactions between the adsorbed particles: (a) multilayer adsorption occurs on heterogeneous surfaces; (b) the amount of the adsorbate depends on the concentration and increases with it; (c) binding sites are occupied gradually, and the strength of the binding decreases with increasing degree of site occupation.

The general nonlinear equations for the Langmuir and the Freundlich models can be expressed as reported in Equations (6) and (7):

$$q_e = \frac{q_M \cdot K_L \cdot C_e}{1 + K_L \cdot C_e} \tag{6}$$

$$q_e = K_F \cdot {C_e}^{1/n} \tag{7}$$

where q_e is the amount of pollutant adsorbed at equilibrium (mg/g), C_e the equilibrium concentration of DCF-Na (mg/L), q_M is the maximum achievable monolayer adsorption capacity (mg/g). K_L, the Langmuir binding constant (L/mg), is related to the adsorption energy of DCF-Na on the surface of hydrogel; whereas K_F (mg/g) is the Freundlich constant, which refers to the adsorption capacity, and $1/n$ is the heterogeneity factor ($1/n > 1$ the adsorption process is unfavorable; $1/n < 1$ the process is favorable).

The Sips isotherm is a three-parameter theoretical model used in the description of adsorption in heterogeneous systems. It is described by the following non-linear Equation (8) in which q_M (mg/g) is the maximum adsorption capacity, K_S (L/mg) is the Sips equilibrium constant, and $1/n$ is the Sips exponent that explains the homogeneity/heterogeneity of the adsorption system.

$$q_e = \frac{q_M \cdot \left(K_S \cdot C_e\right)^{\frac{1}{n}}}{1 + \left(K_S \cdot C_e\right)^{\frac{1}{n}}} \tag{8}$$

When $1/n = 1$ the Sips equation comes down to the Langmuir one (high adsorbate concentration) and the equation predicts a monolayer adsorption, whereas when C_e or K_S are close to 0 the Sips isotherm resembles the Freundlich one.

In Figure 6, the equilibrium adsorption capacity q_e is plotted versus DCF-Na equilibrium concentrations, and the experimental data are fitted with the three isothermal models. The obtained isotherm constants are reported in Table 2, together with the linear correlation coefficients R^2. From the correlation coefficients reported in Table 2, it can be concluded that experimental data fit well both the Langmuir and Sips models ($R^2 > 0.99$). DCF-Na adsorption of LS-pAAm-DAC hydrogel tends to be monolayer, with an almost homogeneous distribution of the contaminant on the surface of the hydrogel. Moreover, the $1/n$ value of 0.714 obtained from the Freundlich model indicates a favorable adsorption process, which means that multilayer adsorption may also

play an important role in the DCF-Na removal from LS-pAAm-DAC (R^2 for Freundlich model is 0.977).

Table 3 presents a comparison of the maximum adsorption capacities of DFC, as predicted by the Langmuir model, across various adsorbents. The adsorption capacity of LS-pAAm-DAC is notable when compared to other natural polymer-based systems [49, 50], carbon-based materials [51, 52], and magnetic nanoparticles [53], although it remains lower than that of some other adsorbents reported in the literature [37, 54].

3.6 | DCF-Na Removal: Packed-Bed Column

The results obtained in the adsorption experiment in batch mode were used to test DCF-Na removal by LS-pAAm-DAC in a packed-bed column from a 43.5 mg/L DCF-Na spiked solution. The collected data are reported in Figure 7 as breakthrough curves with DCF-Na normalized concentration (C/C_0) vs. elution time (t, min) and are further analyzed and fitted with different models [14, 55, 56]. The Thomas model is based on the theory of mass transfer and is used to calculate the maximum adsorption capacity. The analytical relationship representing the model is reported below by Equation (9):

$$\frac{C_t}{C_0} = \frac{1}{1 + e^{K_{TH}\left(\frac{q_e \cdot m}{F} - C_0 t\right)}} \tag{9}$$

where, C_t is the concentration of the diclofenac (mg/L) in the effluent at time t (min), C_0 is DCF-Na initial concentration in the influent (mg/L), K_{TH} is the Thomas constant velocity (mL/(mg min)), F is the flow rate (mL/min), m is the dry hydrogel mass in the column (g), and q_e is the adsorption capacity at the equilibrium (mg/g).

Another model reported in the literature for column adsorption study is the Clark model, whose main assumption is the use of a mass-transfer concept in combination with the Freundlich isotherm and is expressed by Equation (10):

$$\frac{C_t}{C_0} = \frac{1}{\left[1 + Ae^{(-R \cdot t)}\right]^{\frac{1}{n-1}}} \tag{10}$$

TABLE 3 | Comparison of q_M (mg/g) values obtained in DCF adsorption.

Adsorbent	q_M (mg/g)	References
Kaolin-CS-g-poly(AA-co-NIPAM)	18.51	[49]
Guazuma ulmifolia Lam. Fruit	19.7	[50]
Phosphorous-doped microporous carbonous material PPhA	21.11	[51]
Multiwalled carbon nanotubes	7.26	[52]
$Ni_{0.5}Zn_{0.5}Fe_2O_4$ MNPs	52.91	[53]
CPX hydrogel	172.41	[54]
PMA/nMMT hydrogel nanocomposite	152.9	[37]
LS-pAAm-DAC	62.55	This work

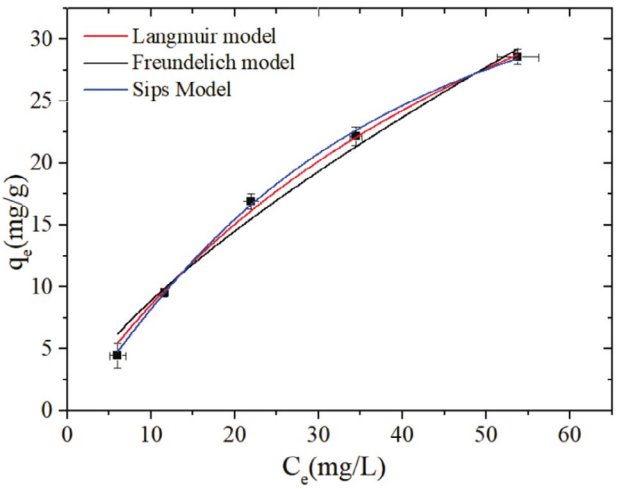

FIGURE 6 | Adsorption isotherm models for DCF-Na batch adsorption by LS-pAAm-DAC.

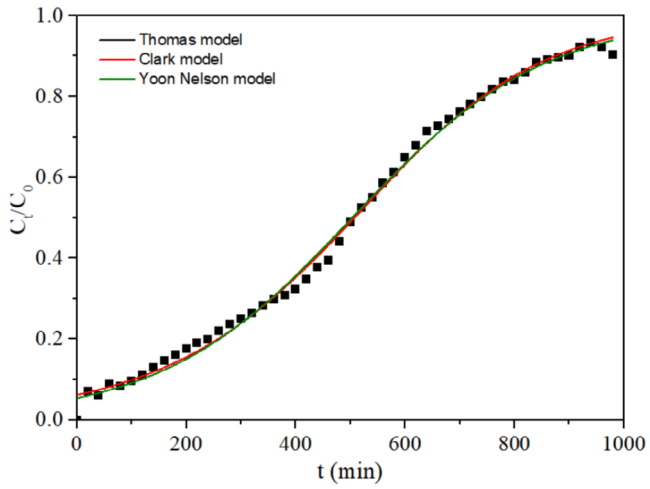

FIGURE 7 | Adsorption isotherm models for DCF-Na adsorption by LS-pAAm-DAC in packed-bed column.

TABLE 2 | Isotherm parameters calculated from Langmuir, Freundlich, Sips models.

Isothermal adsorption models (batch experiments)								
Langmuir			Freundlich			Sips		
q_M (mg/g)	K_L (L/mg)	R^2	K_F (mg/g)	$1/n$	R^2	q_M (mg/g)	K_S (L/mg)	R^2
62.55	0.0156	0.994	1.69	0.714	0.977	42.87	0.0126	0.998

TABLE 4 | Isotherm parameters calculated from Thomas, Clark, and Yoon–Nelson models.

Isothermal adsorption models (packed-bed column)											
Thomas			**Clark**				**Yoon–Nelson**				
$q_{e(exp)}$ (mg/g)	q_e (mg/g)	K_{TH} (mL/mg min)	R^2	A	R (1/min)	$1/n$	R^2	$t_{(exp)}$ (min)	t (min)	K_{YN} (1/min)	R^2
53.4	54.7	0.131	0.996	32.9	0.00622	0.44	0.996	500	503	0.00571	0.996

where C_0 and C_t (mg/L) are DCF-Na concentrations in the influent and in the effluent at time t, respectively, A is the dimensionless Clark constant, R is the Clark constant (1/min), t is the time passed (min), and n is the Freundlich constant. A, R, and n parameters were obtained from the nonlinear regression.

The Yoon and Nelson model is an easy-to-apply model because no detailed data are required regarding the adsorbate, adsorbent, and column properties. It is expressed by the following Equation (11):

$$\frac{C_t}{C_0} = \frac{1}{1 + e^{K_{YN}(\tau - t)}} \tag{11}$$

where C_0 and C_t (mg/L) are DCF-Na concentrations in the influent and in the effluent at time t, respectively, K_{YN} is the constant velocity of Yoon–Nelson (1/min), t and τ are the passed time and the time to reach the breakthrough (min), respectively.

All the three models adequately described the columns' behavior given the same and high correlation coefficients ($R^2 > 0.99$), and the correspondence between the experimental data and the values predicted by the models (q_e for the Thomas model and t for the Yoon–Nelson model), as shown in Table 4.

Moreover, differences were found in the q_e value determined in the column experiment and calculated using the Thomas Model, as well as in the Freundlich constant n, in batch and in column, likely due to different conditions of the two experiments: the concentration gradient at the interface between the solution and the adsorbent in the column is always large, whereas in batch experiments the concentration gradient between the two phases gradually decreases with time [57].

The results obtained are preliminary, and the effects of various parameters—such as initial DCF-Na concentration, flow rate, and bed height—on column performance have yet to be investigated. In addition, the potential for reusing the column in successive cycles remains to be evaluated.

4 | Conclusion

A lignin-based hydrogel containing cationic acryloxy groups (DAC) was synthesized by a radical polymerization, characterized, and tested in the removal of the anti-inflammatory drug DCF-Na. The prepared hydrogel showed efficient adsorption toward DCF-Na in a process in which both physical and chemical interactions may be involved, driven by electrostatic interaction, hydrogen bond, and van der Waals forces. The kinetic data fit well with the pseudo-second-order model, and, as indicated by the intraparticle diffusion model fitting, the process may be governed by multiple steps. Adsorption isotherm models were used to analyze the batch data to obtain the best parameters useful to optimize the process (q_e, K_L, n) and to clarify the mechanism of adsorption, which tends to be monolayer with an almost homogeneous distribution of the contaminant on the surface of the hydrogel. Preliminary packed-bed column adsorption experiments demonstrated the potential of lignin-based hydrogels as effective adsorbent materials for diclofenac (DCF), achieving an adsorption capacity of approximately 54 mg/g. Further experiments, both in batch and column mode, are planned to evaluate the adsorption capacity of these hydrogels not only toward other emerging contaminants such as NSAIDs but also heavy metals, dyes, and endocrine-disrupting compounds. This is made possible by the potential to introduce specific functional groups into the polymeric network, thereby enhancing its affinity toward various contaminants. Hydrogel composites could also be prepared by integrating the hydrogel matrix with other materials, such as nanoparticles or inorganic phases. These additions may synergistically enhance mechanical strength, sorption kinetics, or catalytic activity, thereby opening the door to additional applications.

To sum up, these semisynthetic derivatives may offer a greener alternative to conventional synthetic polymers, thanks to the environmentally friendly nature and low cost of lignin, as well as the hydrogel's intrinsic biocompatibility, water affinity, and degradability. These features reinforce their potential as sustainable and customizable platforms for environmental protection.

Acknowledgments

This research has received funding from the European Union – NextGenerationEU, funded under the National Recovery and Resilience Plan (NRRP), Mission 4 Component 2 Investment 1.5 - 'Creation and strengthening of innovation ecosystems,' construction of 'territorial leaders in R&D' – Innovation Ecosystems - Project 'Innovation, digitalization and sustainability for the diffused economy in Central Italy – VITALITY' —Project Code ECS00000041, CUP I33C22001330007. We acknowledge the Polytechnic University of Marche and MUR for support within the project Vitality.

Conflicts of Interest

The authors declare no conflicts of interest.

Data Availability Statement

Data will be available on request.

References

1. M. O. Barbosa, N. F. F. Moreira, A. R. Ribeiro, M. F. R. Pereira, and A. M. T. Silva, "Occurrence and Removal of Organic Micropollutants: An Overview of the Watch List of EU Decision 2015/495," *Water Research* 94 (2016): 257–279, https://doi.org/10.1016/j.watres.2016.02.047.

2. E. A. Tyumina, G. A. Bazhutin, A. d. P. Cartagena Gómez, and I. B. Ivshina, "Nonsteroidal Anti-Inflammatory Drugs as Emerging Contaminants," *Microbiology* 89 (2020): 148–163, https://doi.org/10.1134/S0026261720020125.

3. M. Ahmaruzzaman, P. Roy, A. Bonilla-Petriciolet, et al., "Polymeric Hydrogels-Based Materials for Wastewater Treatment," *Chemosphere* 331 (2023): 138743, https://doi.org/10.1016/j.chemosphere.2023.138743.

4. A. I. Osman, A. Ayati, M. Farghali, et al., "Advanced Adsorbents for Ibuprofen Removal From Aquatic Environments: A Review," *Environmental Chemistry Letters* 22 (2024): 373–418, https://doi.org/10.1007/s10311-023-01647-6.

5. L. Matêjová, J. Bednárek, J. Tokarský, I. Koutník, B. Sokolová, and G. J. F. Cruz, "Adsorption of the Most Common Non-Steroidal Analgesics From Aquatic Environment on Agricultural Wastes-Based Activated Carbons; Experimental Adsorption Study Supported by Molecular Modeling," *Applied Surface Science* 605 (2022): 154607, https://doi.org/10.1016/j.apsusc.2022.154607.

6. G. Labuto, A. P. Carvalho, A. S. Mestre, et al., "Individual and Competitive Adsorption of Ibuprofen and Caffeine From Primary Sewage Effluent by Yeast-Based Activated Carbon and Magnetic Carbon Nanocomposite," *Sustainable Chemistry and Pharmacy* 28 (2022): 100703, https://doi.org/10.1016/j.scp.2022.100703.

7. M. J. Ahmed, "Adsorption of Non-Steroidal Anti-Inflammatory Drugs From Aqueous Solution Using Activated Carbons: Review," *Journal of Environmental Management* 190 (2017): 274–282, https://doi.org/10.1016/j.jenvman.2016.12.073.

8. S. Akash, B. Sivaprakash, N. Rajamohan, M. Govarthanan, and B. T. Elakiya, "Remediation of Pharmaceutical Pollutants Using Graphene-Based Materials – A Review on Operating Conditions, Mechanism and Toxicology," *Chemosphere* 306 (2022): 135520, https://doi.org/10.1016/j.chemosphere.2022.135520.

9. A. Grela, J. Kuc, and T. Bajda, "A Review on the Application of Zeolites and Mesoporous Silica Materials in the Removal of Non-Steroidal Anti-Inflammatory Drugs and Antibiotics From Water," *Materials* 14 (2021): 4994, https://doi.org/10.3390/ma14174994.

10. S. Lin, Y. Zhao, and Y. S. Yun, "Highly Effective Removal of Non-steroidal Anti-Inflammatory Pharmaceuticals From Water by Zr(IV)-Based Metal-Organic Framework: Adsorption Performance and Mechanisms," *ACS Applied Materials & Interfaces* 10 (2018): 28076–28085, https://doi.org/10.1021/acsami.8b08596.

11. N. Prasetya and C. Wöll, "Removal of Diclofenac by Adsorption Process Studied in Free-Base Porphyrin Zr-Metal Organic Frameworks (Zr-MOFs)," *RSC Advances* 13 (2023): 22998–23009, https://doi.org/10.1039/d3ra03527a.

12. Y. Ngernyen, D. Petsri, K. Sribanthao, et al., "Adsorption of the Non-Steroidal Anti-Inflammatory Drug (Ibuprofen) Onto Biochar and Magnetic Biochar Prepared From Chrysanthemum Waste of the Beverage Industry," *RSC Advances* 13 (2023): 14712–14728, https://doi.org/10.1039/d3ra01949g.

13. A. Michelon, J. Bortoluz, C. S. Raota, and M. Giovanela, "Agro-Industrial Residues as Biosorbents for the Removal of Anti-Inflammatories From Aqueous Matrices: An Overview," *Environmental Advances* 9 (2022): 100261, https://doi.org/10.1016/j.envadv.2022.100261.

14. M. Parlapiano, A. Foglia, M. Sgroi, et al., "Assessment of Molecularly Imprinted Polymers for Selective Removal of Diclofenac From Wastewater by Laboratory and Pilot-Scale Adsorption Tests," *Journal of Water Process Engineering* 63 (2024): 105467, https://doi.org/10.1016/j.jwpe.2024.105467.

15. M. Parlapiano, C. Akyol, A. Foglia, et al., "Selective Removal of Contaminants of Emerging Concern (CECs) From Urban Water Cycle via Molecularly Imprinted Polymers (MIPs): Potential of Upscaling and Enabling Reclaimed Water Reuse," *Journal of Environmental Chemical Engineering* 9 (2021): 105051, https://doi.org/10.1016/j.jece.2021.105051.

16. Y. Xu, Z. Fan, X. Li, et al., "Cooperative Production of Monophenolic Chemicals and Carbon Adsorption Materials From Cascade Pyrolysis of Acid Hydrolysis Lignin," *Bioresource Technology* 399 (2024): 130557, https://doi.org/10.1016/j.biortech.2024.130557.

17. D. Rico-Garcìa, L. Ruiz-Rubio, L. Pérez-Alvarez, S. L. Hernàndez-Olmos, G. L. Guerrero-Ramiréz, and L. V. Vilas-Vilela, "Lignin-Based Hydrogels: Synthesis and Applications," *Polymers* 12 (2020): 81, https://doi.org/10.3390/polym12010081.

18. S. Thakur, P. P. Govender, M. A. Mamo, S. Tamulevicius, Y. K. Mishra, and V. K. Thakur, "Progress in Lignin Hydrogels and Nanocomposites for Water Purification: Future Perspectives," *Vacuum* 146 (2017): 342–355, https://doi.org/10.1016/j.vacuum.2017.08.011.

19. S. Wang, X. Chen, Y. Yin, et al., "Lignin-Based Hydrogels for Efficient Dye Removal via Synergistic Effect of Multiple Interactions," *Industrial Crops and Products* 189 (2022): 115840, https://doi.org/10.1016/j.indcrop.2022.115840.

20. S. Wei, W. Chen, Z. Tong, N. Jiang, and M. Zhu, "Synthesis of a Functional Biomass Lignin-Based Hydrogel With High Swelling and Adsorption Capability Towards Acid Red 73," *Environmental Science and Pollution Research* 28 (2021): 51306–51320, https://doi.org/10.1007/s11356-021-14324-4.

21. Y. Liu, Y. Cui, G. Wu, and M. Liao, "Preparation and Properties of Fast Temperature-Responsive Soy Protein/PNIPAAm IPN Hydrogels," *Journal of the Serbian Chemical Society* 79 (2014): 211–224, https://doi.org/10.2298/JSC130219047L.

22. S. Qian, F. Zhang, B. Liu, H. Ren, and G. Tong, "Polyacrylate-Based Water-Absorbent Hydrogels Prepared With Lignin-Related Compounds: Process Conditions and Performance," *BioResources* 12, no. 3 (2017): 6607–6661.

23. A. Zerpa, L. Pakzad, and P. Fatehi, "Hardwood Kraft Lignin-Based Hydrogels: Production and Performance," *ACS Omega* 3 (2018): 8233–8242, https://doi.org/10.1021/acsomega.8b01176.

24. A. Onder, P. Ilgin, H. Ozay, and O. Ozay, "Removal of Dye From Aqueous Medium With pH-Sensitive Poly[2-(Acryloyloxy)ethyl]Trimethylammonium Chloride-Co-1-Vinyl-2-Pyrrolidone Cationic Hydrogel," *Journal of Environmental Chemical Engineering* 8 (2020): 104436, https://doi.org/10.1016/j.jece.2020.104436.

25. S. L. Banerjee, T. Swift, R. Hoskins, S. Rimmer, and N. K. Singha, "A Muscle Mimetic Polyelectrolyte-Nanoclay Organic-Inorganic Hybrid Hydrogel: Its Self-Healing, Shape-Memory and Actuation Properties," *Journal of Materials Chemistry B* 7 (2019): 1475–1493, https://doi.org/10.1039/c8tb02852d.

26. J. T. Price, W. Gao, and P. Fatehi, "Lignin-g-Poly(Acrylamide)-g-Poly(Diallyldimethyl-Ammonium Chloride): Synthesis, Characterization and Applications," *ChemistryOpen* 7 (2018): 645–658, https://doi.org/10.1002/open.201800105.

27. A. Steudel, F. Friedrich, W. Lieske, et al., "Simultaneous Thermal Analysis of Cationic, Nonionic and Anionic Polyacrylamide," *Heliyon* 5 (2019): e02973, https://doi.org/10.1016/j.heliyon.2019.e02973.

28. H. Taghavian and S. R. M. Reza, "Investigation of the Effects of Starch on the Physical and Biological Properties of Polyacrylamide (PAAm)/Starch Nanofibers," *Progress in Biomaterials* 6 (2017): 85–96, https://doi.org/10.1007/s40204-017-0069-7.

29. Y. Liu, H. Zheng, Y. Wang, et al., "Synthesis of a Cationic Polyacrylamide by a Photocatalytic Surface-Initiated Method and Evaluation of Its Flocculation and Dewatering Performance: Nano-TiO2 as a Photo Initiator," *RSC Advances* 8 (2018): 28329–28340, https://doi.org/10.1039/c8ra05622f.

30. X. Zhang, M. Han, A. Fuseni, and A. M. Alsofi, "An Approach to Evaluate Polyacrylamide-Type Polymers' Long-Term Stability Under High Temperature and High Salinity Environment," *Journal of Petroleum Science and Engineering* 180 (2019): 518–525, https://doi.org/10.1016/j.petrol.2019.04.092.

31. M. E. S. R. Silva, E. R. Dutra, V. Mano, and J. C. Machado, "Preparation and Thermal Study of Polymers Derived From Acrylamide," *Polymer Degradation and Stability* 67 (2000): 491–495, https://doi.org/10.1016/S0141-3910(99)00149-4.

32. I. Neamtu, A. P. Chiriac, L. Nita, G. Ghica, and V. Alley, "Characterization of Poly(Acrylamide) as Temperature-Sensitive Hydrogel," *Journal of Optoelectronics and Advanced Materials* 8 (2006): 1939–1943.

33. M. Khan, L. A. Shah, J. Fu, F. Ning, and H. M. Yoo, "Ultra-Adhesive Iontronic Hydrogels Strengthened by Folded Protein for Flexible Transducer With Language Recognition Capabilities," *Chemical Engineering Journal* 504 (2025): 159008, https://doi.org/10.1016/j.cej.2024.159008.

34. A. Nimra, M. Sher, M. Khan, L. A. Shah, J. Fu, and E. A. Ali, "Ex Situ Synergistic Reinforcement of a MOF-Based Supramolecular Polymer Enables Tough, Highly Flexible, and Responsive Artificial Epidermis-Inspired Hydrogels," *Journal of Materials Chemistry C* 13 (2025): 5041–5055, https://doi.org/10.1039/D4TC05163G.

35. Y. Liu, Y. Wang, Y. Fu, et al., "Healable and Transparent Ionic Conductive Hydrogels Based on PNATF as Multiple-Signal Sensors," *ACS Applied Polymer Materials* 7 (2025): 2529–2540, https://doi.org/10.1021/acsapm.4c03794.

36. Y. Liu, Y. Wang, Y. Fu, et al., "Fabrication of Temperature and pH Dual-Sensitive Semi-Interpenetrating Network Hydrogel With Enhanced Adhesion and Antibacterial Properties," *Polymer* 326 (2025): 128343, https://doi.org/10.1016/j.polymer.2025.128343.

37. S. A. Khan, M. F. Siddiqui, and T. A. Khan, "Synthesis of Poly(Methacrylic Acid)/Montmorillonite Hydrogel Nanocomposite for Efficient Adsorption of Amoxicillin and Diclofenac From Aqueous Environment: Kinetic, Isotherm, Reusability, and Thermodynamic Investigations," *ACS Omega* 5 (2020): 2843–2855, https://doi.org/10.1021/acsomega.9b03617.

38. L. Ai, M. Li, and L. Li, "Adsorption of Methylene Blue From Aqueous Solution With Activated Carbon/Cobalt Ferrite/Alginate Composite Beads: Kinetics, Isotherms, and Thermodynamics," *Journal of Chemical & Engineering Data* 56 (2011): 3475–3483, https://doi.org/10.1021/je200536h.

39. Y. Meng, J. Lu, Y. Cheng, Q. Li, and H. Wang, "International Journal of Biological Macromolecules Lignin-Based Hydrogels: A Review of Preparation, Properties, and Application," *International Journal of Biological Macromololecules* 135 (2019): 1006–1019, https://doi.org/10.1016/j.ijbiomac.2019.05.198.

40. W. Zhang, L. Hu, S. Hu, and Y. Liu, "Optimized Synthesis of Novel Hydrogel for the Adsorption of Copper and Cobalt Ions in Wastewater," *RSC Advances* 9 (2019): 16058–16068, https://doi.org/10.1039/c9ra00227h.

41. S. Şahin and S. Emik, "Fast and Highly Efficient Removal of 2,4-D Using Amino-Functionalized Poly (Glycidyl Methacrylate) Adsorbent: Optimization, Equilibrium, Kinetic and Thermodynamic Studies," *Journal of Molecular Liquids* 260 (2018): 195–202, https://doi.org/10.1016/j.molliq.2018.03.091.

42. P. Moharrami, S. Hazratic, F. Shakeri, E. Motamedi, and S. Ariaeenejad, "Sodium Alginate- and Chitosan-Based Hydrogels With Different Network Charges for Selective Removal of Cationic and Anionic Dyes From Water," *Water Quality Research Journal* 59 (2024): 205–222, https://doi.org/10.2166/wqrj.2024.008.

43. I. M. Ibrahim, M. A. Radwan, M. A. Sadek, S. A. Darwish, and N. Y. Mostaf, "Effect of Electrostatic Interactions on the Dye Removal Behavior of Different Hydrogel-Based Materials," *Egyptian Journal of Chemistry* 66 (2023): 257–261, https://doi.org/10.21608/EJCHEM.2022.176630.7228.

44. W. He, Y. Wang, X. Li, et al., "Sealing the Pandora's Vase of Pancreatic Fistula Through Entrapping the Digestive Enzymes Within a Dextrorotary (D)-Peptide Hydrogel," *Nature Communications* 15, no. 1 (2024): 7235, https://doi.org/10.1038/s41467-024-51734-7.

45. J. Wang and X. Guo, "Adsorption Kinetic Models: Physical Meanings, Applications, and Solving Methods," *Journal of Hazardous Materials* 390 (2020): 122156, https://doi.org/10.1016/j.jhazmat.2020.122156.

46. Y. V. Vaganov, M. A. Kadyrov, D. A. Drugov, and O. A. Tugushev, "Contaminated Water Flow Modelling Through the Porous Media by Using Fractional Advection-Dispersion Equation (FADE)," *Geology, Ecology, and Landscapes* 8, no. 4 (2023): 489–497, https://doi.org/10.1080/24749508.2022.2154924.

47. J. O. Ighalo and A. G. Adeniyi, "Adsorption of Pollutants by Plant Bark Derived Adsorbents: An Empirical Review," *Journal of Water Process Engineering* 35 (2020): 101228, https://doi.org/10.1016/j.jwpe.2020.101228.

48. R. Saadi, Z. Saadi, R. Fazaeli, and N. E. Fard, "Monolayer and Multilayer Adsorption Isotherm Models for Sorption From Aqueous Media," *Korean Journal of Chemical Engineering* 32 (2015): 787–799, https://doi.org/10.1007/s11814-015-0053-7.

49. A. R. Abdullah and L. S. Jasim, "High-Efficiency Removal of Diclofenac Sodium (DS) Drug Using Chitosan-Grafted-Poly(Acrylic Acid-Co-N-Isopropylacrylamide)/Kaolin Clay Hydrogel Composite," *International Journal of Environmental Analytical Chemistry* (2024): 1–21, https://doi.org/10.1080/03067319.2024.2361335.

50. L. A. Araujo, C. O. Bezerra, L. F. Cusioli, M. T. Rodríguez, R. G. Gomes, and R. Bergamasco, "Diclofenac Adsorption Using a Low-Cost Adsorbent Derived From *Guazuma Ulmifolia* Lam. Fruit via Chemical and Thermal Treatment," *Journal of Environmental Chemical Engineering* 9 (2021): 106629, https://doi.org/10.1016/j.jece.2021.106629.

51. M. T. Sekulic, N. Boskovic, A. Slavkovic, J. Garunovic, S. Kolakovic, and S. Pap, "Surface Functionalised Adsorbent for Emerging Pharmaceutical Removal: Adsorption Performance and Mechanisms," *Process Safety and Environmental Protection* 125 (2019): 50–63, https://doi.org/10.1016/j.psep.2019.03.007.

52. A. Gila, L. Santamaría, and S. A. Korili, "Removal of Caffeine and Diclofenac From Aqueous Solution by Adsorption on Multiwalled Carbon Nanotubes," *Colloid and Interface Science Communications* 22 (2018): 25–28, https://doi.org/10.1016/j.colcom.2017.11.007.

53. Z. Mohammadi, A. R. Kelishami, and A. Ashrafi, "Application of $Ni_{0.5}Zn_{0.5}Fe_2O_4$ Magnetic Nanoparticles for Diclofenac Adsorption: Isotherm, Kinetic and Thermodynamic Investigation," *Water Science and Technology* 83, no. 6 (2021): 1265–1277, https://doi.org/10.2166/wst.2021.049.

54. M. Chelu, M. Popa, J. Calderon Moreno, et al., "Green Synthesis of Hydrogel-Based Adsorbent Material for the Effective Removal of Diclofenac Sodium From Wastewater," *Gels* 9 (2023): 454, https://doi.org/10.3390/gels906045.

55. H. Patel, "Fixed-Bed Column Adsorption Study: A Comprehensive Review," *Applied Water Science* 9 (2019): 45, https://doi.org/10.1007/s13201-019-0927-7.

56. H. Patel, "Comparison of Batch and Fixed Bed Column Adsorption: A Critical Review," *International Journal of Environmental Science and Technology* 19 (2022): 10409–10426, https://doi.org/10.1007/s13762-021-03492-y.

57. V. K. Gupta and I. Ali, "Removal of Lead and Chromium From Wastewater Using Bagasse Fly Ash—A Sugar Industry Waste," *Water Research* 35 (2001): 33–40, https://doi.org/10.1016/j.jcis.2003.11.007.

Supporting Information

Additional supporting information can be found online in the Supporting Information section.